Publ. Astron. Soc. Japan **40**, 459–474 (1988)

Continuum Observation of Sagittarius B2 at 23 and 43 GHz

Kenji AKABANE,* Yoshiaki SOFUE,† Hisashi HIRABAYASHI,
Masaki MORIMOTO, and Makoto INOUE

Nobeyama Radio Observatory,§ Minamimaki-mura, Minamisaku-gun, Nagano 384-13

and

Dennis DOWNES

Institut de Radio Astronomie Millimetrique, Voie 10, Domaine Universitaire de Grenoble, 38406 Saint-Martin-D'Heres Cedex, France

(Received 1987 November 6; accepted 1988 March 24)

Abstract

The source Sgr B2 has been mapped with a single-dish resolution of $\sim 40''$ at frequencies of 23 GHz and 43 GHz ($\lambda = 1.3$ cm and 6.9 mm respectively). An extended thermal component was found, and has been compared with that in lower frequency observations. The core region of Sgr B2 (containing the compact sources MD4 and MD5) was resolved at both 23 GHz and 43 GHz. The compact components MD4 and MD5 have complex thermal spectra which may indicate inhomogeneities within each compact core. A new source, G0.64−0.06, was found in the southern area of the extended thermal component. The 43-GHz map made with the Nobeyama 45-m telescope was also convolved to an angular resolution of 1′.3, for comparison with a 10.7-GHz map made with the Effelsberg 100-m telescope. This comparison suggests that there may be some nonthermal emission in the southern area of Sgr B2.

Key words: H II regions; Nonthermal sources; Radio continuum radiation.

1. Introduction

The H II region called Sgr B2 is one of the most impressive sources near the center of the Galaxy, and numerous interstellar molecules have been discovered in the clouds associated with Sgr B2.

Early radio continuum observations of the Sgr B2 region were summarized by Downes and Maxwell (1966), and subsequent studies have been made by many workers,

* Present address: Department of Physics, Faculty of Science, Toyama University, Toyama 930.

† Present address: Institute of Astronomy, The University of Tokyo, Mitaka, Tokyo 181.

§ Nobeyama Radio Observatory is a branch of the National Astronomical Observatry, an inter-university research institute operated by the Ministry of Education, Science, and Cutture.

including high resoltution observations with interferometers operating at centimeter wavelengths (Martin and Downes 1972; Balick and Sanders 1974; Downes et al. 1978; Benson and Johnston 1984; Garay et al. 1985; Roelfsema et al. 1987; Vogel et al. 1987). However, as yet, relatively few observations of this region have been made with single dishes with resolutions of $<1'$ in the shorter centimeter-wavelength range.

An optically thin thermal spectrum of the region with a spectral index of -0.1 to -0.2 was evident from investigations at wavelengths of 2–10 cm (Downes and Maxwell 1966), but recent shorter-wavelengths results do not lie on a simple extrapolation of this spectrum. Data from Hobbs and Johnston (1971) suggested a steep downturn of the spectrum for frequencies ≥ 18 GHz, while integrated flux densities in the 3-mm band greatly exceeded the centimeter flux levels (Hobbs et al. 1971; Righini et al. 1976). A millimeter-wave excess relative to the homogeneous free-free thermal emission seen at lower frequencies was discussed in terms of contributions from a dense dust cloud (Righini et al. 1976), as well as from ionized clouds of high elecron density (Hobbs et al. 1971).

In this paper, we present single-dish observations of the Sgr B2 region with 40″ resolutions at 23 and 43 GHz, made with the Effelsberg 100-m and the Nobeyama 45-m telescopes respectively. The aims of these observations were (1) a morphological study of the region to find the spectral characteristics of the central compact sources and the associated extended component, and (2) surface brightness measurements to search for evidence for millimeter-wave excess emission as claimed by Hobbs et al. (1971), Righini et al. (1976), and Akabane et al. (1986), or for brightness decreases which would suggest the presence of nonthermal sources, possibly supernova remnants, in the region around Sgr B2.

2. Observations

2.1. *Effelsberg Observations*

The 23-GHz observations were made with the Effelsberg 100-m telescope in April–June 1976, in clear weather, at night. The mixer receiver had a center frequency of 22.8 GHz ($\lambda=1.31$ cm), a system temperature of 500 to 700 K (DSB) and an I.F. bandwidth of 450 MHz. The half-power beamwidth was $39''\times 43''$ (azimuth$\times$elevation), independent of elevation. The source NGC 7027 was used as a primary calibrator, with an assumed flux density of 5.9 Jy at 23 GHz. The source NRAO 530 was used for pointing checks, giving an accurarcy of 3″ throughout the observations.

At 22.8 GHz, the aperture efficiency was 25% in the zenith relative to the inner 80-m diameter of the dish, which has a solid surface, rather than open mesh. This corresponds to a response (S/T) of 2.2 Jy K^{-1} for a point source in the zenith. At an elevation of 10°, the aperture efficiency of the inner 80-m of the dish was 16% and the main-beam efficiency was 35%. The area mapped was from R.A. $17^h43^m40^s$ to $17^h44^m40^s$, Decl. $-28°19'$ to $-28°27'$. The telescope was held stationary to exclude variations in sky temperature and ground radiation during any scan. In total, 25 drift scans were made per map, spaced every 20″ in declination, with an integration time constant of 0.″25. The maps were repeated five times, to achieve a final sensitivity of 0.05 K r.m.s. on the summed map. The corrections for atmospheric extinction

for each night of observing were estimated from observations of the moon, NGC 7027, 3C 84, 3C 273 and 3C 279 at various elevations. A typical value for the zenith optical depth was 0.15.

2.2. Nobeyama Observations

The 43-GHz observations were made in May and June 1985 as part of the radio continuum survey of galactic sources at NRO, and were successfully done for the two source regions Sgr A and Sgr B2 on two clear nights. The 45-m telescope was equipped with a Schottky-barrier diode-mixer receiver combined with a parametric amplifier, both being cooled at the 20-K stage of a liquid helium refrigerator. The center frequency and bandwidth were 43.25 GHz and 0.5 GHz respectively, and the system temperature was about 500 K at the zenith. Only one linear polarization was detected, which was fixed with the elevation angle of the telescope. A beam switching mode was employed in which the main beam was switched at a frequency of about 20 Hz to a reference beam separated by about 6′ in azimuth from the main beam. The full width to half power at the main beam was 39″, and the reference beamwidth was almost identical. The beam-switching system of the NRO 45-m dish will be described elsewhere.

The mapping was done by scanning the region in galactic latitude, over an area of $\Delta l \times \Delta b = 10' \times 10'$ centered at $(\alpha, \delta) = 17^{h}44^{m}10^{s}.6$, $-28°22'05''$ (1950.0). The area was covered with 40 scans in total, in steps of 15″ in Δl, but an effective area of $\Delta l \times \Delta b = 8' \times 8'$ was actually available for the present study, given the rather close separation of the reference beam.

The flux densities were calibrated relative to maps of the source NGC 7027, obtained just after the observations of Sgr B2. The flux density of NGC 7027 at 43.25 GHz was taken to be 6.0 ± 0.3 Jy, by extrapolating the spectrum determined by Harris and Scott (1976), as was also done for the map of the Sgr A region by Sofue et al. (1986). The observed peak flux density of Sgr B2, which occurs at the position of the compact source MD5 of Martin and Downes (1972), was 17 Jy/(39″ beam area) ($=6.1 \times 10\ \mathrm{W\ m^{-2}\ Hz^{-1}\ sr^{-1}} = 10.5\ \mathrm{K}\ T_b$). The source was assumed to be unpolarized in this band. The pointing accuracy was estimated to be better than $\pm 15''$ in the mapped region.

Confusion from molecular line emission in the 500-MHz continuum bandwidth observed here, such as the 43.12-GHz SiO maser line, is negligibly small (less than 0.002 K of T_b; private communication from N. Ukita, M. Ohishi, and T. Hasegawa).

The 43-GHz data were reduced with the CONDUCT astronomical reduction system at NRO, and scanning effects on the map were removed with the pressing method (Sofue and Reich 1979).

The beam shape, measured by mapping 3C 273, was almost circular to half maximum. The strongest side lobes were 20 dB below the peak of main beam.

3. Observational Results

The 23-GHz map of the Sgr B2 region obtained at 40″ resolution with the Effelsberg

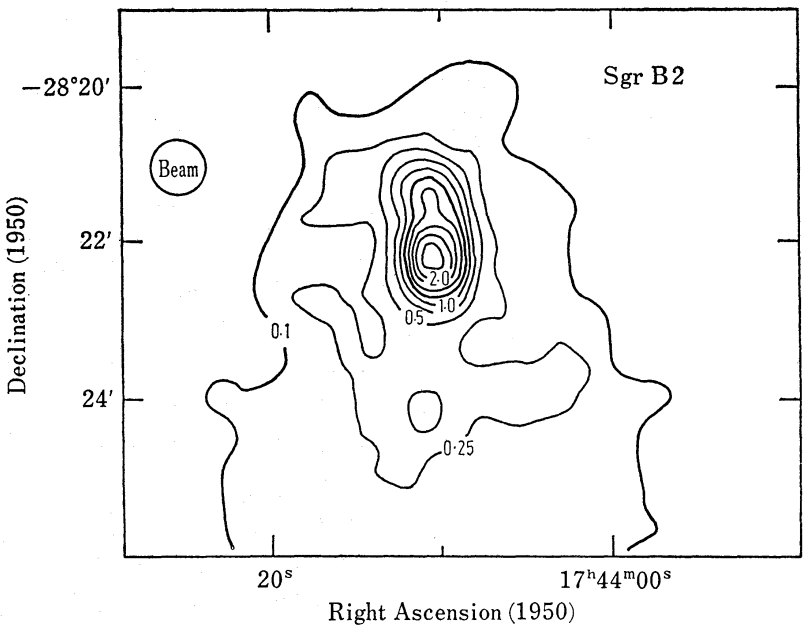

Fig. 1. Effelsberg radio continuum map of the Sgr B2 region at 22.8 GHz. Beam=40″, contour unit=6.125 K, and main-beam T_b=4.23 Jy/(40″ beam).

100-m telescope is shown in figure 1. The 43-GHz map of almost the same region, with 39″ resolution, by the Nobeyama 45-m telescope is shown in figure 2. In both maps, the region is resolved into several sources and each source is accompanied by an extended component which is usually not detected in interferometer observations. The positions, half-widths, and intensities of individual sources were derived from cross-cuts of intensity vs. position on the contour maps. Most of resolved sources can be identified with MD sources (Martin and Downes 1972). Figure 3 is an example of a cross-cut, showing sources MD4 and MD5. The sources MD3, MD6, and MD7 around MD4 and MD5 are not resolved in the present 23-GHz and 43-GHz observations.

The diffuse or extended component is numbered as (3) in figure 3. We assumed this component to have a single structure as indicated by the broken line in the figure, although each individual source may have its own respective background component. Most single-dish observations at centimeter wavelengths so far have not shown the structure of this extended component, because of the low resolutions used ($\sim 2'$) and the rather strong nonthermal ridge component. In previous millimeter observations with single dishes, this extended component may have been confused with the core, because of the low signal-to-noise ratios. High-resolution interferometers may not be appropriate to detect this sort of extended component, because of the missing information at short spacings.

Parameters of the observed sources are listed in tables 1 and 2 for 23 GHz and 43 GHz respectively. Source 6, G0.64−0.06, in figure 2 and in table 2 was not seen in the interferometer observations by Martin and Downes (1972); the source seems to be extended.

A brief description of this region at 43 GHz was also reported by Hirabayashi et al. (1987). They investigated a difference in the spectra of the northern and southern

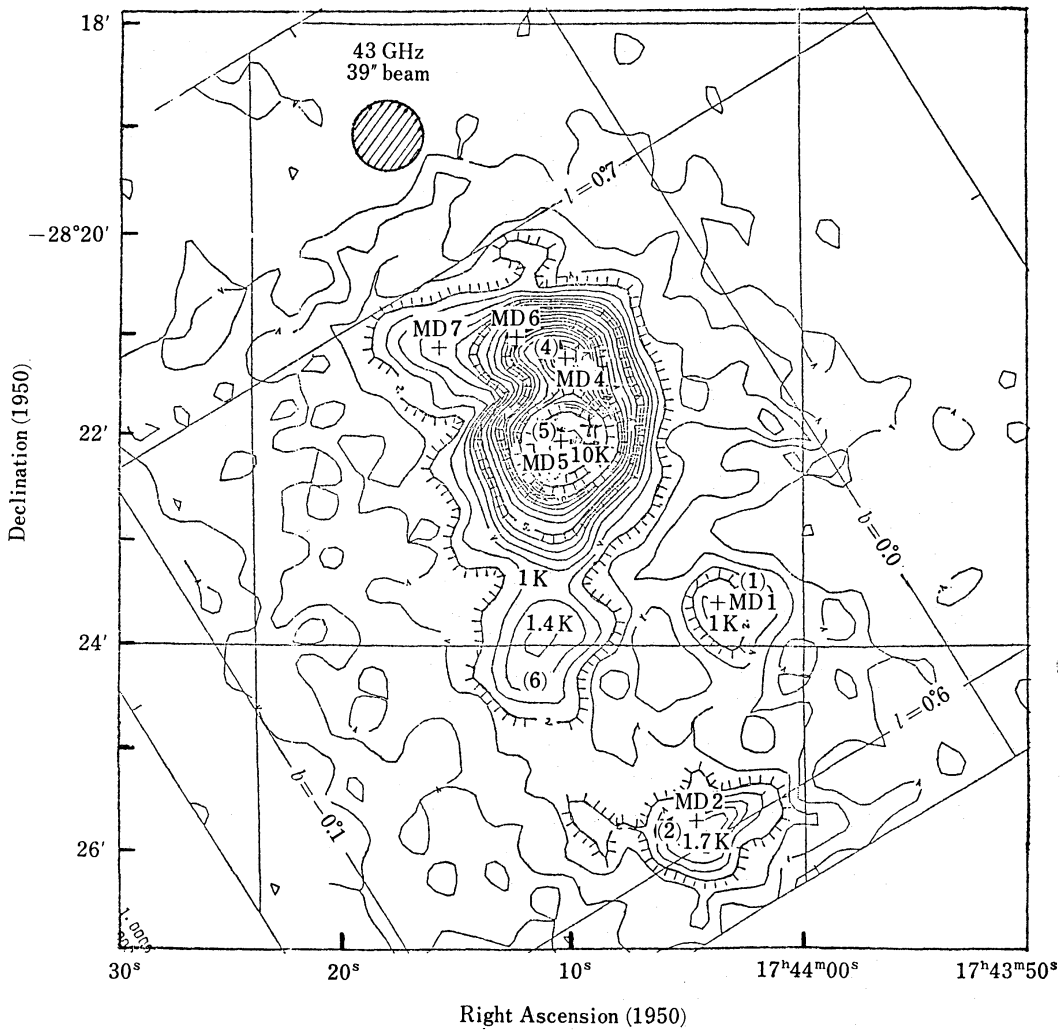

Fig. 2. Nobeyama radio continuum map of the Sgr B2 region at 43 GHz, beam=39″ circular, contour unit=0.42 K, main-beam T_b=0.68 Jy/(39″ beam area at 43 GHz), and peak contour T_b=10.5 K. Numbers in parentheses correspond to the source numbers in table 2.

Table 1. Source parameters from the 23-GHz Effelsberg map of the Sgr B2 region.

Source name	Peak position		Observed width	Peak intensity from model fit			Integrated flux (Jy)
	R.A. (1950)	Decl. (1950)	R.A.× Decl.	(map units)	(K T_b)	(Jy/40″ beam)	
MD4	17ʰ44ᵐ11ˢ.0	−28°21′15″	47″×40″	1.05	6.43	4.44	5.25
MD5	17 44 10.5	−28 22 10	42″×62″	2.37	14.52	10.03	16.32

Total flux in the whole map=72 Jy (extended component: about 50 Jy).

Conversion factors: 1 map unit=6.125 K T_b=4.23 Jy/(40″ beam), calculated for a wavelength of 1.31 cm.

extended areas of the region, and proposed, as a working model of the source, that the southern area may have some nonthermal emission.

Comparisons between typical cross-cuts of the 23-GHz and 43-GHz maps have

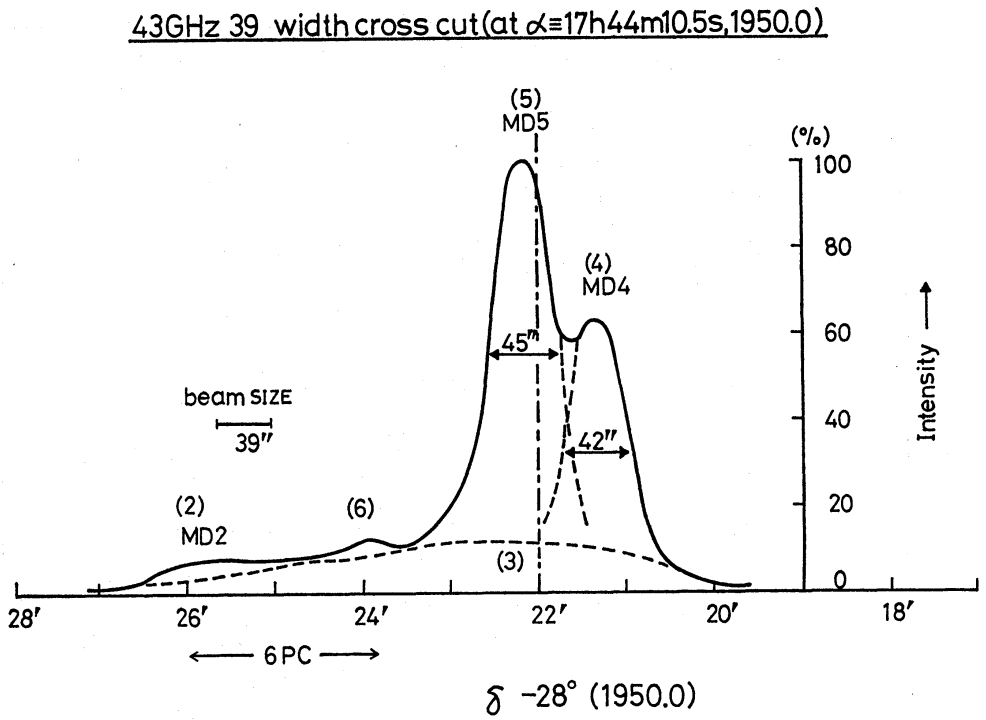

Fig. 3. An example of a cross-cut in declination at 43 GHz, through the peaks of MD4 and MD5 (Downes et al. 1978). The profile consists of several resolved components, labeled by the source numbers given in table 2.

Table 2. Source parameters from the 43-GHz Nobeyama map of an 8′×8′ (R.A.×Decl.) region around Sgr B2.

No.	Source name	Peak position (1950.0)	Observed width R.A.×Decl.	Peak intensity	Total flux density	Remarks
(1)	MD1	$\alpha=17^h44^m3^s.5$ $\delta=-28°23'45''$	~47″×~47″	1.2 Jy/39″ beam	1.7±0.5 Jy	
(2)	MD2	$\alpha=17^h44^m4^s.5$ $\delta=-28°25'50''$	~67″×~48″	2.3 Jy/39″ beam	4.9±1 Jy	
(3)	Extended	$\alpha=17^h44^m10^s$ $\delta=-28°23'0''$	~4′ ×~4′	1.9 Jy/39″ beam	71±20 Jy	
(4)	MD4	$\alpha=17^h44^m10^s.6$ $\delta=-28°21'20''$	~45″×~42″	10.9 Jy/39″ beam	11±5 Jy	
(5)	MD5	$\alpha=17^h44^m10^s.5$ $\delta=-28°22'20''$	~45″×~45″	17 Jy/39″ beam	20±7 Jy	
(6)	G0.64−0.06	$\alpha=17^h44^m11^s.8$ $\delta=-28°24'10''$	~65″×~70″	1.9 Jy/39″ beam	5.3±2 Jy	Not seen in MD sources
(7)	H II total	...	...	...	114±30 Jy	

The components are derived from cross-cuts, as shown in figure 3. MD3, MD6, and MD7 (Martin and Downes 1972) are barely resolved in the present 43-GHz observation, as can be seen in the map of figure 2.

been made, and three of them are given in figures 4, 5, and 6. The relative intensity of each cross-cut was normalized to the peak intensity of MD5 in each map. We see, for source 6 in figure 4, a new source G0.64−0.06, which is also visible in figures 1

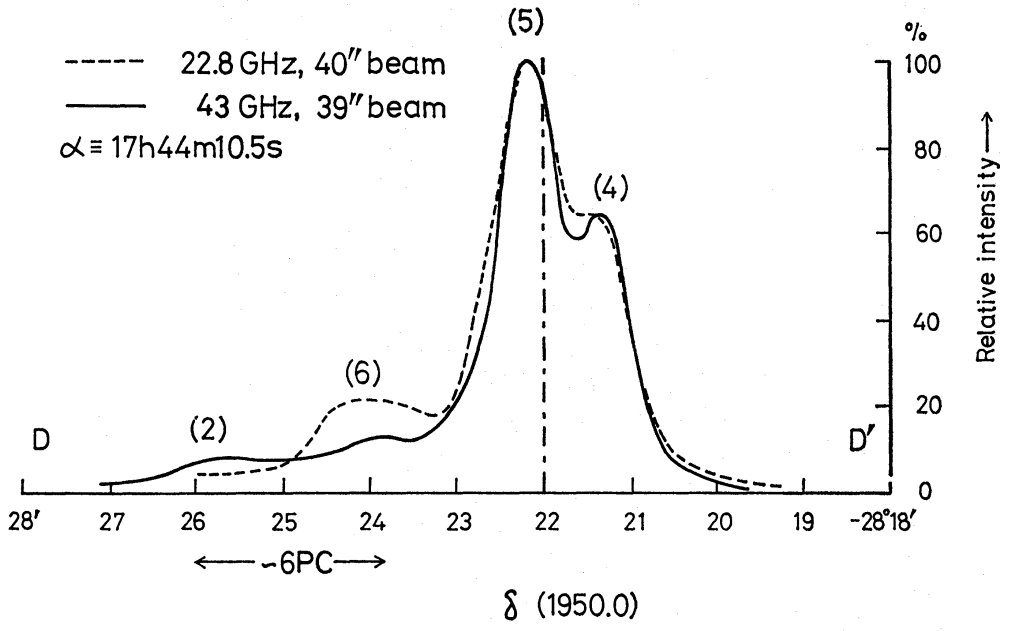

Fig. 4. Cross-cuts in declination, at R.A. = $17^h44^m10^s.5$, through the 23- and 43-GHz maps of figures 1 and 2. The peak intensity of each cross-cut is normalized to 100% at the peak of MD5. Numbers along profiles are source numbers as listed in table 2.

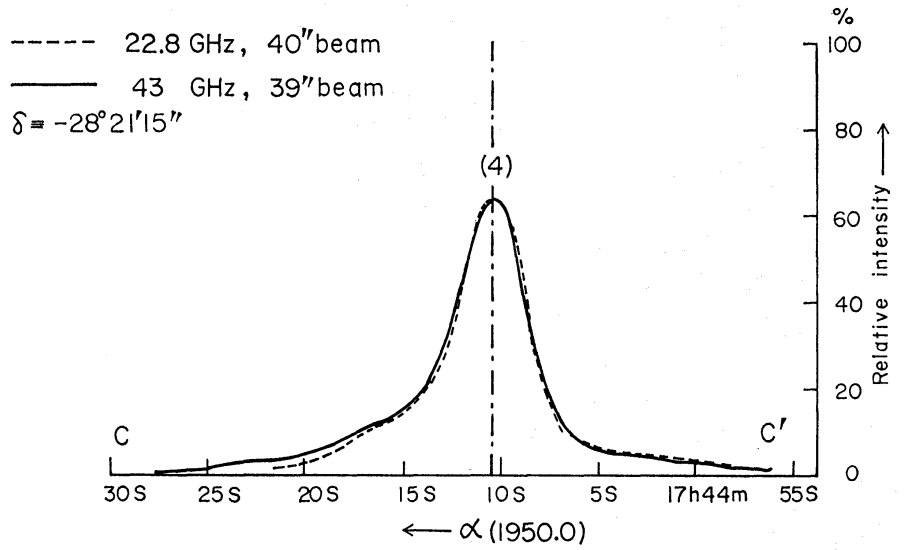

Fig. 5. Cross-cuts in right ascension, at Decl. = −28°21′15″, through the peak of MD 4, from the 23- and 43-GHz maps of figures 1 and 2. As in figure 4, the intensity of each profile is normalized, so that it would reach 100% at the peak of MD5. The peak of MD4 is labeled by (4).

and 2 and listed in table 2 as source 6. Figure 5 shows that the cross-cuts at both frequencies coincide very well, as would be expected for optically thin thermal emission due to free-free transitions. The cross-cuts in figures 4 and 6, however, show some increments of the 23-GHz intensities above those at 43 GHz, depending upon the positions in the cross-cut profiles. The intensity increments at 23 GHz, as in regions

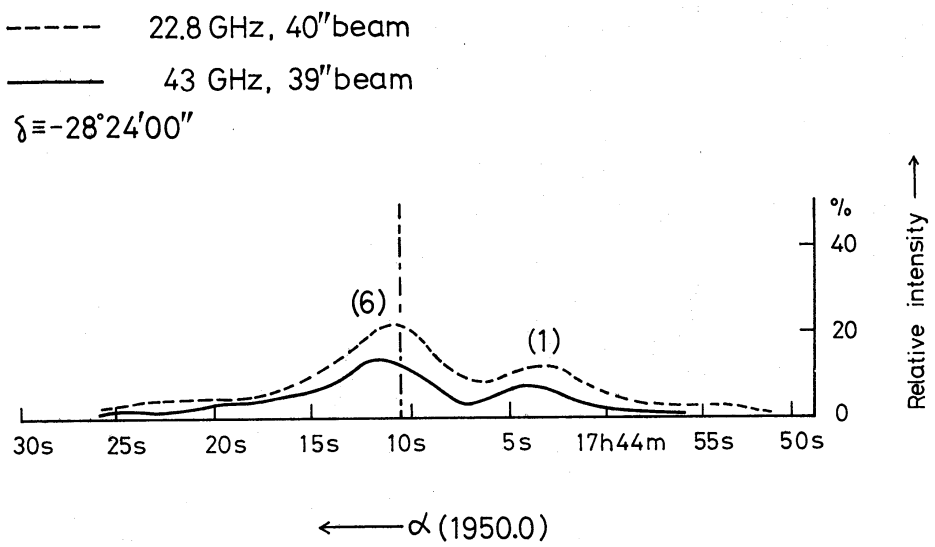

Fig. 6. Cross-cuts in right ascension, at Decl. $=28°24'00''$ through the 23- and 43-GHz maps of figures 1 and 2. As in figures 4 and 5, the intensity of each cross-cut is normalized, so that 100% corresponds to the peak of MD5. Source numbers (1) and (6) in table 2 are labeled at the positions in the profiles.

1 and 6 in figure 6, may suggest the presence of nonthermal emission in the extended area of the Sgr B2 region.

4. Radio Spectrum of the Sgr B2 Region

Flux densities of the central core and the total area, obtained from the 40″ resolution maps, are plotted in figure 7 together with centimeter- and millimeter-wave results obtained by previous workers. To interpret figure 7, we take two groups of data points, labeled A and B in the figure, as a working model, where group A is for the total flux densities of the region, while group B includes the flux density of the core component only, obtained from high-resolution single-dish observations at 10.7 GHz by Downes et al. (1978) (indicated by ○), at 23 GHz by the Effelsberg 100-m telescope (indicated by ⊞), and at 43 GHz by the Nobeyama 45-m telescope (indicatd by ⊕). We assumed that the low values for the fluxes at 11.1 GHz and 18.2 GHz (Hobbs and Johnston 1971) are due to low estimates of the extended component of the source in their maps. This was pointed out by Kapitzky and Dent (1974) in their 15.5-GHz observation of the Sgr B2 region. In fact, observations at 10.7 GHz (Downes et al. 1978) as well as the present 23- and 43-GHz data show an observed half maximum width of about $4' \times 4'$(R.A. $\times$ Decl.) for the extended component, suggesting that the actual area of the extended distribution is about $10' \times 10'$. This should be kept in mind for high sensitivity, full surveys of the region. We assume here that the total, but lower intensities published by other workers around 10 GHz to 30 GHz correspond to those of the core component seen at Effelsberg and Nobeyama, plotted at 10.7 GHz, 23 GHz, and 43 GHz in the figure. As a working hypothesis, we presume that some of the data in group B include a small fraction of the flux from the extended component.

The treatment of integrated flux densities in figure 7 is similar to that in figure 10

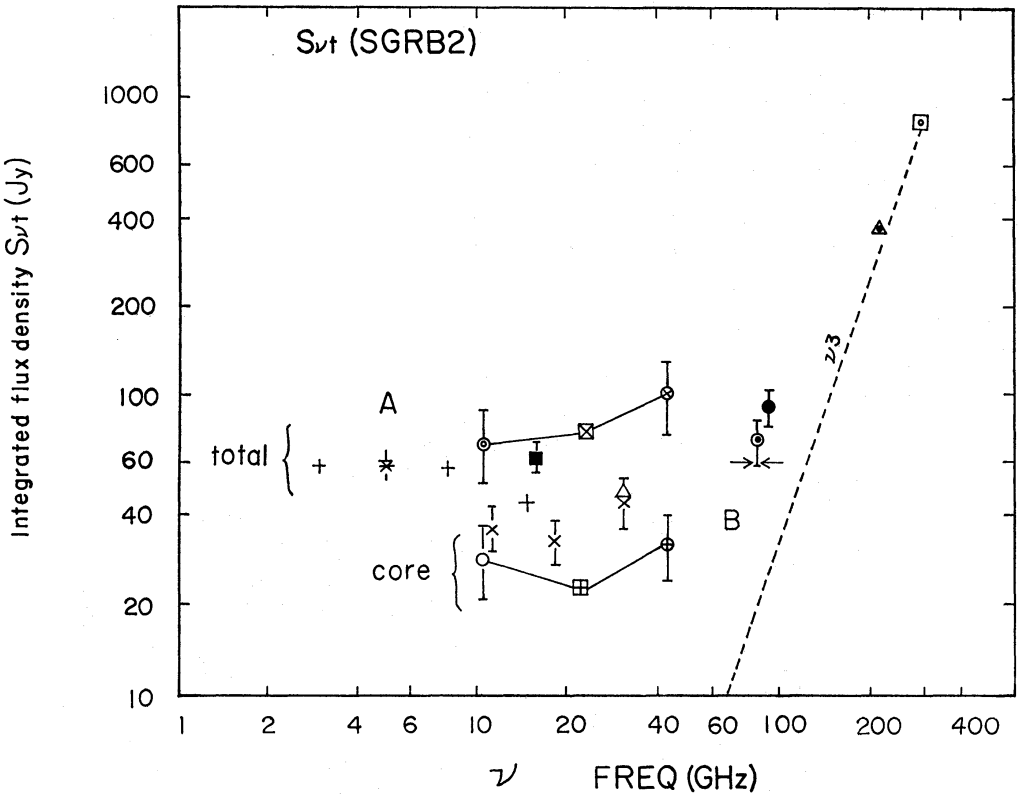

Fig. 7. Integrated flux densities ($S_{\nu t}$) in the centimeter and millimeter ranges. Data are labeled as follows: +: Downes and Maxwell 1966, ∗: Altenhoff et al. 1978, ×: Hobbs and Johnston 1971, △: Downes et al. 1970, ⊙: Hobbs et al. 1971, ●: Righini et al. 1976, ■: Kapitzky and Dent 1974, ◬: Clegg et al. 1974, and ⊡: Westbrook et al. 1976. The symbols ◎ and ○ are for the total and the central compact component, respectively, from the 10.7-GHz map by Downes et al. (1978). The symbols (⊠, ⊞) and (⊗, ⊕) are for the present 23-GHz and 43-GHz observations, and for the flux densities of the total area and of the central core component respectively. Arrows at 84.2 GHz show a new result by Gordon et al. (1986).

by Downes et al. (1978), which also summarized flux densities within different areas of the extended source.

In group A, the integrated flux density of the whole region might be measured more reliably in the decimeter and centimeter range than in the millimeter range, due to better signal-to-noise ratio, even though the beamwidths are nearly the same.

As we see in figure 7, the toal intensity of 43 GHz at Nobeyama is fairly large, compared with fluxes at other frequencies. We checked carefully our intensity calibration during the observations with a new type of beam-switching system at the 45-m telescope. A large error in intensity could come from the estimated extent of the diffuse component. There seems to be a trend for the integrated flux densities to increase with frequency in the millimeter-wave region in both groups A and B in the figure. A possible contribution from the dust grain emission in the millimeter-wave region is represented in the figure by a function increasing with frequency, ν, as ν^3, and which is equal to the values measured at wavelengths of 1 mm and 1.4 mm (Westbrook et al. 1976; Clegg et al. 1974).

5. The Core Component of Sgr B2

The observed core components at 23 GHz and 43 GHz are shown in figures 1 and 2 as the two close discrete sources MD4 and MD5; the source parameters are listed in tables 1 and 2. From the observed profiles, such as in figures 3 and 4, we estimated upper limits to the angular sizes of the sources to be $<20''$ for MD4 and $<10''$ for MD5 in both right ascension and declination. The symbols w_1 and x_1 in figure 8a represent flux densities, from this paper, of MD4 at 23 and 43 GHz, and w_2 and x_2 in figure 8b represent the fluxes of MD5 at 23 and 43 GHz respectively. Interferometer results are reproduced as t_1, u_1, and v_1 for MD4 in figure 8a, and as t_2, u_2, and v_2, for MD5 (+MD3) in figure 8b. Apparent spectral discontinuities are seen from w_1 to x_1 in figure 8a and from v_2 to w_2 in figure 8b. A reasonable, optically

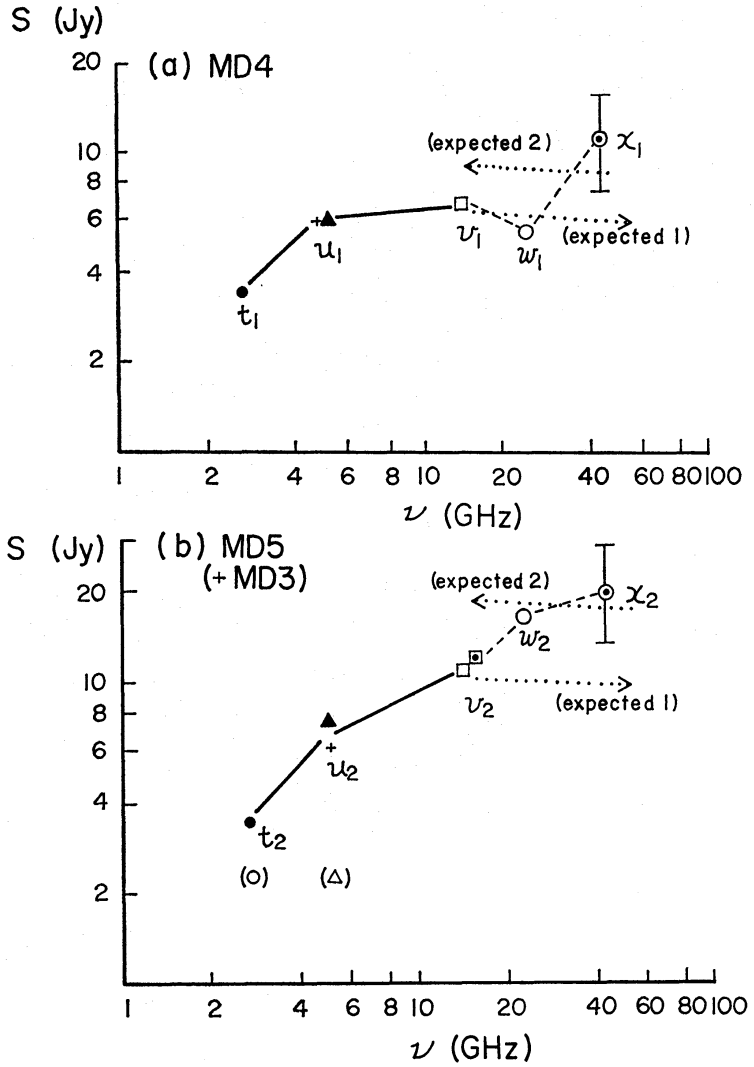

Fig. 8. Flux densities of MD 4, in (a: upper part), and MD 5, in (b: lower part), in the 2.7-GHz to 43-GHz range. Interferometer data are from Balick and Sanders (1974) as ●, Martin and Downes (1972) as ○ and △, Benson and Johnston (1984) as ⊡ and +, Downes et al. (1978) as ▲, and Garay et al. (1985) as □. The symbols ○ and ⊙ are for the present 23-GHz and 43-GHz observations respectively.

thin, free-free thermal spectrum can be found for each of MD4 and MD5, if we presume that part of the flux density measured with single dishes could come from a larger-scale structure around each compact source, which is missing in the interferometer observations. However, the observed turnover of the thermal spectra appears to be very broad, especially for MD5 in figure 8b, where the turnover covers 3 to 40 GHz. If this very broad turnover is real, then parts of the source must be optically thick even at 40 GHz, suggesting either (a) a complex distribution of the electron density within the compact source, which would yield a broad distribution of turnover frequencies, or (b) a complex distribution of the dust emission around and within the compact H II region, which makes an increasing contribution to the flux densities measured at higher frequencies.

If the source MD4 has roughly a flat spectrum in the 5- to 40-GHz range, as indicated in figure 8a, then the excess of the total flux density of the region at 43 GHz, as seen in figure 7 (group A or B), will be partly due to the flux increase of MD5, where part of the source may still be optically thick, even at 43 GHz. As with some stellar wind sources with radial variations in electron density, the flux density of MD5 seems to increase with frequency as $\sim\nu^{0.7}$, but not as ν^2. The flat spectra, which would be expected for MD4 and MD5, if they were both homogeneous and optically thin, are shown by dotted lines labeled "expected 1" and "expected 2" in figures 8a and 8b, where we postulate overestimates of the flux densities in the millimeter range (curve labeled "expected 1"), and underestimates from the interferometer observations (curve labeled "expected 2").

6. The Extended Component of Sgr B2

Another component, surrounding the core component, is shown in figure 3, as the broken line labeled (3) [it is also listed as (3) in table 2]. This component seems to be physically associated with MD4, MD5, and other discrete sources in the region. The structure of this component could not be deduced from previous low-resolution ($\sim 2'$) single-dish observations in the centimeter range because of confusion with the non-thermal component, which dominates the emission along the galactic equator.

Figure 9 shows the new data from the 23- and 43-GHz observations, together with best estimates of the flux of the extended component in Sgr B2 from previous observations. The spectrum appears to be thermal, except for an up-turn near 43 GHz. However, this up-turn of the intensity in the millimeter range might be evidence that the component contains a contribution from dust emission. The flux density increases from ~ 40 Jy to ~ 70 Jy in the frequency range 5 GHz to 43 GHz, although the observational error is large. If the source is thermal, a simple estimate shows a quite low electron density within this component, roughly a tenth of that of Orion A or W3, whereas the electron densities of the regions MD4 and MD5 are about ten times as large as in the Orion A region. This large contrast in electron density between the core and the extended components suggests that the extended component may be a region ionized by a large association of earlier generations of OB stars whose H II regions have by now expanded to larger sizes and lower densities. This difference in ages and masses of the exciting stars would explain why MD4 and MD5 appear to be

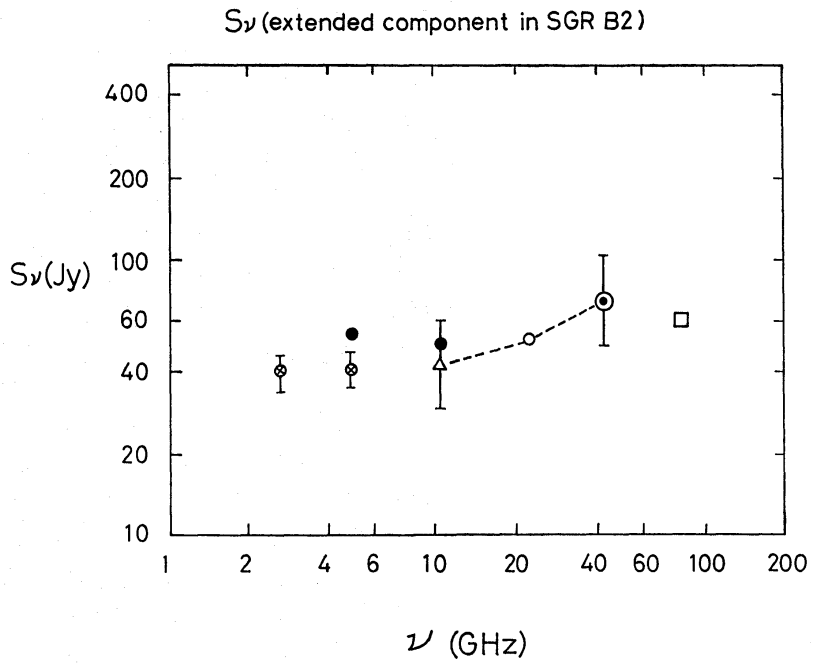

Fig. 9. Spectrum of the flux densities of the extended component of Sgr B2 region. In the figure, data from Martin and Downes (1972) are marked as ⊗, and from Downes et al. (1978) as filled circles. The open triangle is for the present estimate from the 10.7 GHz map by Downes et al. (1978), and the open square gives the result by Righini et al. (1976). The open circle and the circle with central dot are for the 23-GHz and 43-GHz data, respectively, as given in tables 1 and 2.

well-developed, high-density and intense H II regions, in contrast with the much weaker structures of the extended component, whose total flux density is quite large, about twice that of the core component. Other possibilities may be contributions to the total flux of the extended component by old supernova remnants, or by weaker ionization from many protostars just starting to contribute Lyman photons or ionizing winds to the region. It is also suggestive that the background structure as seen in figures 1 and 2 resembles that seen at 1 mm by Westbrook et al. (1976) and at 350 μm by Righini et al. (1975), especially with regard to the extensions to the northeast in the area around MD6 and MD7.

7. Comparison with the Bonn 10.7-GHz Map

As discussed in the previous sections, Sgr B2 region has been resolved into several sources, including an extended one, with a single-dish resolution of around 40″ at wavelengths of 7 and 13 mm. A few, weak, nonthermal sources may be present in the southern area of the region. To obtain the frequency spectrum of the extended component, possibly including some of the weak unresolved sources, the 43-GHz map was compared with the 10.7-GHz map of the region made at Effelsberg. For this comparison, the Nobeyama 43-GHz map was reconvolved by computer to have an angular resolution of 1′.3 as in the case of 10.7-GHz observation by the 100-m telescope. The 10.7-GHz map is reproduced here from the work by Downes et al. (1978). The 43-

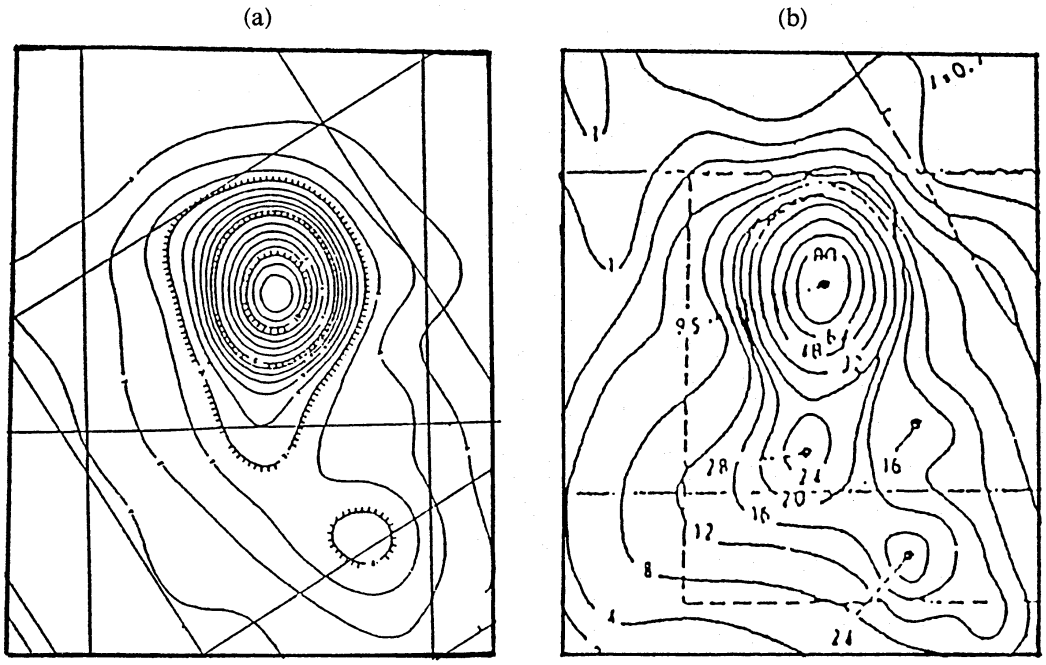

Fig. 10. Intensity maps of Sgr B2 region at an angular resolution of 1'.3. (a) is the 43-GHz map convolved by computer from the original 39″ resolution of the 45-m telescope at Nobeyama, and (b) is the 10.7-GHz map from the 100-m telescope (Downes et al. 1978).

GHz and 10.7-GHz maps of the region thus obtained are shown in figures 10a and 10b respectively. From the two maps, we see that the southern part is more intense and extended at 10.7 GHz than at 43 GHz, indicating the possible existence of a non-thermal component. Figure 11a shows declination cross-cuts at R.A.$=17^{h}44^{m}10^{s}.5$, from the maps of figures 10a and 10b, with the peak intensities of the cross-cuts normalized to be 100%. The positions were adjusted by $<10''$ (noted as X-Y in the figure) to have the peaks coincide.

This procedure was done under the assumption that the core component of the region has an optically thin thermal spectrum in this frequency range. Figure 11b shows the percentage difference, ΔI, between the 10.7- and 43-GHz intensity contours of figure 11a. Figure 11b shows a clear excess of 10.7-GHz intensity over that at 43 GHz in the southern area of the region, noted by (A) in the figure, whereas in the northern part of the region, the 10.7-GHz excess is not evident; there may be a decrement indicated by (B) in the figure. The localized peak of the 10.7-GHz cross-cut at around Decl.$=-28°24'20''$ may correspond to the source 6, G0.64−0.06, in table 2.

For comparison, figure 11 shows normalized cross-cuts obtained with almost the same spatial resolution, 1'.2, at millimeter wavelengths, namely the 93.0-GHz result by Righini et al. (1976) and the 84.2-GHz result by Gordon et al. (1986). Again, we see the excess of the 10.7-GHz emission above the millimeter emission in the southern part of the source region.

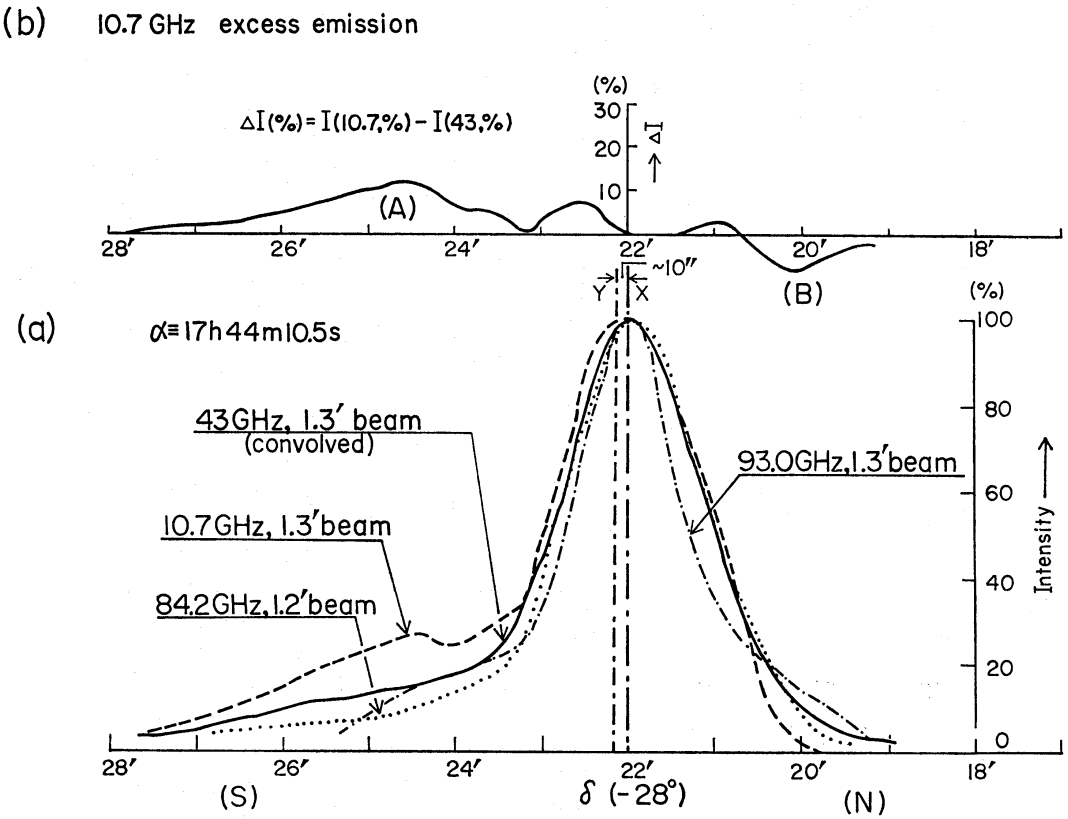

Fig. 11. Declination cross-cuts from the maps in figures 10a and b through the peaks of MD4 and MD5, at R.A.=$17^h44^m10^s.5$. Figure (a) also includes the corresponding cross-cuts from the 84.2-GHz map by Gordon et al. (1986) and from the 93.0-GHz map by Righini et al. (1976). The percentage intensity difference, $\Delta I(\%)$, between the cross-cuts at 10.7 GHz and 43 GHz is given in figure b, at the top of the figure.

The intensity difference between the 10.7-GHz and 43-GHz contours (ΔI in figure 11b) is shown as a contour map in figure 12. In the figure, the region is roughly separated into two areas of $\Delta I>0$ and of $\Delta I<0$ as denoted by A and B respectively in the figure. In region A ($\Delta I>0$), there may be four localizations of ΔI at a, b, c, and d, corresponding to the continuum source positions 5, 4, 6, and 2 in table 2 respectively; the peaks in ΔI are nearly associated with, but not coincident with, the continuum sources in table 2. In region B ($\Delta I<0$), two peaks are seen, labeled e and f, in an elongated shell structure which appears to surround source 4, MD4, but there are no continuum sources coincident with peaks e and f.

Figures 11 and 12 are based on the assumption that the core region near MD4 and MD5 is optically thin at frequencies higher than 10 GHz. However, it is also possible that parts of the core region may still be optically thick, above 10 GHz, as suggested by the curves in figures 8a and 8b for MD4 and MD5 respectively.

8. Conclusions

The Sgr B2 region was resolved with the single-dish resolution of ~40″ at 23 GHz and 43 GHz. The resolved sources in the core region were identified with the sources

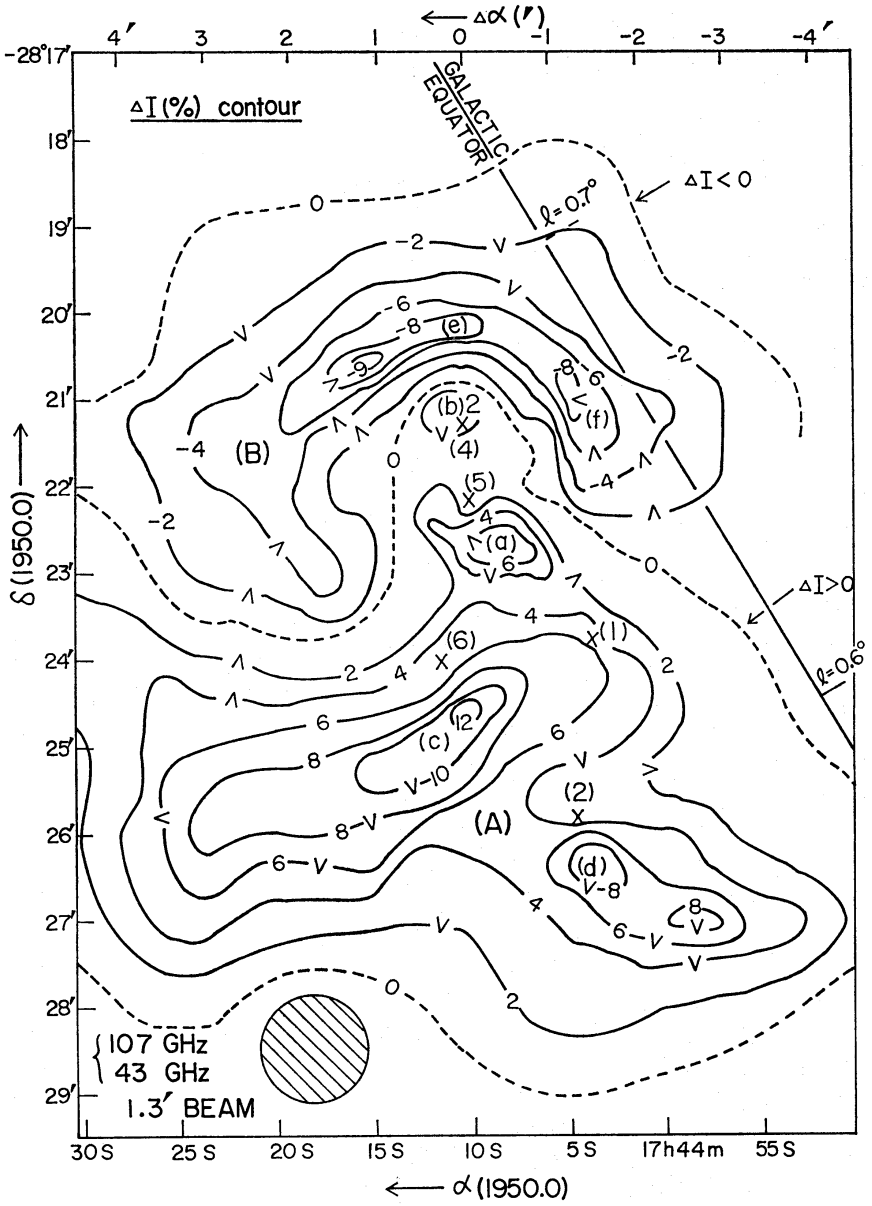

Fig. 12. Map of 10.7-GHz excess (ΔI in Fig. 11) relative to the 43-GHz intensity. Contour numbers are percentages, normalized to 100% at the peak of MD5, where both intensities are assumed to be the same. The region seems to be divided into two areas of $\Delta I>0$ and $\Delta I<0$, marked as (A) and (B), respectively, in the figure.

MD4 and MD5, and the spectrum of each source indicates a complex structure within the compact source itself. That is, there is no simple turnover point in their thermal spectra, at short centimeter wavelengths. The flux density of each source increases as $\sim\nu^{0.3-0.7}$, and not as ν^2, with frequency. This increase of the flux density over a wide range of frequency may imply that each compact source itself consists of complex H II clouds, some of which are optically thin and others which are optically thick. For a better understanding of the spectra of the sources MD4 and MD5, we must be able to separate the flux density of the nearby extended component from that of each

compact source. The extended component observed here is clearly a different one from the nonthermal galactic ridge component, which is presumably synchrotron emission, and is known to be quite intense in the decimeter wavelength range. The extended component which we observe is probably associated with the core of Sgr B2, and has primarily a thermal spectrum. However, a comparison of the brightness in the 43- and 10.7-GHz maps suggests that there may be a few weak nonthermal sources in the southern part of the extended region. In this area, a newly identified source, G0.64−0.06, may be nonthermal; it is probably extended, as it did not appear in the interferometer survey by Martin and Downes (1972). It may be a supernova remnant associated with the strong H II region MD5.

The authors are grateful to the NRO engineers and operators for their collaboration and for the computer reduction, and to A.H.M. Martin for help with the 23-GHz observations. The authors also thank Miss A. Ide for her work on the drawings and the manuscript. The 43-GHz observation is part of the NRO continuum project, for which the Orion A and W3 regions have already been published (Akabane et al. 1986, 1987).

References

Akabane, K., Hirabayashi, H., and Sofue, Y. 1986, *Publ. Astron. Soc. Japan*, **38**, 775.
Akabane, K., Hirabayashi, H., and Sofue, Y. 1987, in *Star Forming Regions, IAU Symp. No. 115*, ed. M. Peimbert and J. Jugaku (D. Reidel Publishing Company, Dordrecht), p. 167.
Akabane, K., Sofue, Y., Hirabayashi, H., and Inoue, M. 1985, *Publ. Astron. Soc. Japan*, **37**, 123.
Altenhoff, W. J., Downes, D., Pauls, T., and Schraml, J. 1978, *Astron. Astrophys. Suppl.*, **35**, 23.
Balick, B., and Sanders, R. H. 1974, *Astrophys. J.*, **192**, 325.
Benson, J. M., and Johnston, K. J. 1984, *Astrophys. J.*, **277**, 181.
Clegg, P. E., Ade, P. A. R., and Rowan-Robinson, M. 1974, *Nature*, **249**, 530.
Downes, D., Goss, W. M., Schwarz, U. J., and Wouterloot, J. G. A. 1978, *Astron. Astrophys. Suppl.*, **35**, 1.
Downes, D., and Maxwell, A. 1966, *Astrophys. J.*, **146**, 653.
Downes, D., Maxwell, A., and Rinehart, R. 1970, *Astrophys. J. Letters*, **161**, L123.
Garay, G., Reid, M. J., and Moran, J. M. 1985, *Astrophys. J.*, **289**, 681.
Gordon, M. A., Jewell, P. R., Kaftan-Kassim, M. A., and Salter, C. J. 1986, *Astrophys. J.*, **308**, 288.
Harris, S., and Scott, P. F. 1976, *Monthly Notices Roy. Astron. Soc.*, **175**, 371.
Hirabayashi, H., Akabane, K., Morimoto, M., Sofue, Y., Inoue, M., and Handa, T. 1987, in *Star Forming Regions, IAU Symp. No. 115*, ed. M. Peimbert and J. Jugaku (D. Reidel Publishing Company, Dordrecht), p. 158.
Hobbs, R. W., and Johnston, K. J. 1971, *Astrophys. J.*, **163**, 299.
Hobbs, R. W., Modali, S. B., and Maran, S. P. 1971, *Astrophys. J. Letters*, **165**, L87.
Kapitzky, J. E., and Dent, W. A. 1974, *Astrophys. J.*, **188**, 27.
Martin, A. H. M., and Downes, D. 1972, *Astrophys. Letters*, **11**, 219.
Righini, G., Simon, M., Joyce, R. R. 1976, *Astrophys. J.*, **207**, 119.
Righini, G., Simon, M., Joyce, R. R., and Gezari, D. Y. 1975, *Astrophys. J. Letters*, **195**, L77.
Roelfsema, P. R., Goss, W. M., Whiteoak, J. B., Gardner, F, F., and Pankonin, V. 1987, *Astron. Astrophys.*, **175**, 219.
Sofue, Y., Inoue, M., Handa, T., Tsuboi, M., Hirabayashi, H., Morimoto, M., and Akabane, K. 1986, *Publ. Astron. Soc. Japan*, **38**, 475.
Sofue, Y., and Reich, W. 1979, *Astron. Astrophys. Suppl.*, **38**, 251.
Vogel, S. N., Genzel, R., and Palmer, P. 1987, *Astrophys. J.*, **316**, 243.
Westbrook, W. E., Werner, M. W., Elias, J. H., Gezari, D. Y., Hauser, M. G., Lo, K. Y., and Neugebauer, G. 1976, *Astrophys. J.*, **209**, 94.